ADVANCED ELECTRONIC MATERIALS Open Access
www.advelectronicmat.de

Improving Charge Transport and Environmental Stability of Carbohydrate-Bearing Semiconducting Polymers in Organic Field-Effect Transistors

*Madison Mooney, Lauren Pandolfi, Yunfei Wang, Chenhui Zhu, Garima Garg, Ulrike Kraft, Xiaodan Gu, and Simon Rondeau-Gagné**

Semiconducting polymers offer synthetic tunability, good mechanical properties, and biocompatibility, enabling the development of soft technologies previously inaccessible. Side-chain engineering is a versatile approach for optimizing these semiconducting materials, but minor modifications can significantly impact material properties and device performance. Carbohydrate side chains have been previously introduced to improve the solubility of semiconducting polymers in greener solvents. Despite this achievement, these materials exhibit suboptimal performance and stability in field-effect transistors. In this work, structure–property relationships are explored to enhance the device performance of carbohydrate-bearing semiconducting polymers. Toward this objective, a series of isoindigo-based polymers with carbohydrate side chains of varied carbon-spacer lengths is developed. Material and device characterizations reveal the effects of side chain composition on solid-state packing and device performance. With this new design, charge mobility is improved by up to three orders of magnitude compared to the previous studies. Processing–property relationships are also established by modulating annealing conditions and evaluating device stability upon air exposure. Notably, incidental oxygen-doping effects lead to increased charge mobility after 10 days of exposure to ambient air, correlated with decreased contact resistance. Bias stress stability is also evaluated. This work highlights the importance of understanding structure–property relationships toward the optimization of device performance.

1. Introduction

Research in organic semiconductors plays a crucial role in the development of next-generation electronics as emerging devices often require enhanced versatility and tunability to interact in original ways with the human body and the environment.[1–3] The development of electronic devices with applications in personalized healthcare, energy production, and smart packaging rely not only on high-performance materials, but also the enabling of innovative properties such as stretchability, improved mechanical endurance, and biocompatibility.[4–7] Semiconducting polymers (SPs) have a strong potential for use in next-generation electronics due to their solution processability and synthetic tunability.[8,9] Previous advancements in this field have unveiled SPs with self-healing properties, high charge transport, and intrinsic stretchability for a wide variety of applications.[10–13] Properties such as solvent resistance, thermochromism or solvatochromism have further diversified the applicability of SPs in sensors and diagnostic technologies.[14–18] Despite these many exciting developments, commercialization of next-generation organic electronics remains a challenge. Industrial scale-up, batch-to-batch variation and stability in environmental conditions are all key challenges that often need to be addressed for the commercialization of organic electronic devices.[19,20] Investigating structure-processing-property relationships is, thus,

M. Mooney, L. Pandolfi, G. Garg, S. Rondeau-Gagné
Department of Chemistry and Biochemistry
University of Windsor
Windsor, Ontario N9B 3P4, Canada
E-mail: srondeau@uwindsor.ca

The ORCID identification number(s) for the author(s) of this article can be found under https://doi.org/10.1002/aelm.202400537

DOI: 10.1002/aelm.202400537

Y. Wang, X. Gu
School of Polymer Science and Engineering
The University of Southern Mississippi
Hattiesburg, MS 39406, USA

C. Zhu
Advanced Light Source
Lawrence Berkeley National Laboratory
Berkeley, CA 94720, USA

U. Kraft
Organic Bioelectronics Research Group
Max Planck Institute for Polymer Research
55182 Mainz, Germany

necessary to bridge the gap to commercialization of high-performance SPs and expand the use of these emerging devices in various fields.

A deeper understanding of the relationship between material structure, processing, and device properties is critical for the development of next-generation organic electronics. Manipulation of structure-property relationships has led to the design and preparation of high-performance SPs with charge mobilities in organic field-effect transistors (OFETs) often surpassing 10 cm^2 V^{-1} s^{-1}.[21,22] In π-conjugated SPs, chemical design strategies such as side chain engineering or backbone modification have been shown to have significant and predictable impacts on device performance properties.[23–25] However, processing conditions, i.e., the experimental conditions used to process the active materials in the functional devices, can also substantially influence charge transport properties by directly impacting thin film morphology and interlayer compatibility.[26,27] Therefore, as highlighted often in the literature, it is imperative to consider not only structure–property relationships in the design of a new semiconducting materials, but also the impact of synthetic design on processing parameters.[20] For example, Di et al. used a solvent-assisted reannealing post-treatment to improve molecular packing of several SPs, resulting in a threefold improvement of charge mobility in OFETs.[28] Chaudhary and colleagues also showed that, by simply modifying solvent selection and using an off-centered spin coating technique, a 50-fold increase in charge mobility in OFETs could be achieved for poly(3-hexylthiophene) (P3HT), which was attributed to the generation of highly ordered crystalline nanowires.[29] These approaches, among many others, demonstrate that the investigation of structure-processing-property relationships is crucial to the development of high-performance materials.

Previously, we synthesized a series of isoindigo-based SPs with carbohydrate side chains to improve processability in ecofriendly solvents.[30] By varying the ratio of carbohydrate-bearing block in a statistical random copolymer (from 20 to 80 mol%), we were able to tune the solubility of the polymers and achieve processability in a *n*-butanol/*o*-anisole solvent mixture, a greener alternative to typically-used halogenated solvents. The materials were directly investigated in OFETs to evaluate the greener processing conditions and their impact on device characteristics. We found that the performance of the carbohydrate-containing polymers was comparable to that of a reference polymer bearing only branched alkyl side chains. Furthermore, device performance was maintained in devices processed from the green solvent blend. In a later study, we found that, by increasing the ratio of carbohydrate-bearing block (80 and 100 mol%) and using a more rigid donor monomer, triggered solvent-resistance could be achieved through intermolecular hydrogen bonding of the carbohydrate side chains.[31] OFETs fabricated from these polymers using *o*-anisole showed no loss of performance, and good film quality was observed after solvent-resistance had been triggered or after subsequent submersion in a variety of solvents. Overall, while these polymers possess exciting properties for the green processing of semiconducting polymers and triggered solvent-resistance for additive manufacturing of organic electronics, they demonstrated relatively low charge mobilities in OFETs (around 10^{-4} cm^2 V^{-1} s^{-1}), presenting a critical barrier to their expansion and application in functional devices.

In this work, we address that challenge by exploring the structure-processing-property relationships of a new series of carbohydrate-bearing SPs. Additionally, investigation of the environmental stability of these polymers in OFETs was undertaken to evaluate this critical property for broad application and future commercialization of related technologies. Adapting previously reported synthetic procedures, we report the synthesis and characterization of a series of isoindigo-based SPs that exhibit significantly improved electronic properties by varying several key structural and processing parameters. In particular, the length of the galactose-terminated side chain was modified to investigate the impact on solid-state properties and charge transport.[24,32] The monomers were also copolymerized with a bithiophene donor unit.[33] Upon structural characterization of the new polymer series, charge transport properties were investigated in OFETs. A meticulous structural characterization of the new polymer series was performed using atomic force microscopy (AFM) and grazing incidence wide-angle X-ray scattering (GIWAXS) to evaluate the solid-state properties of the new materials. These findings were then closely correlated to device performance, probed through the fabrication of OFETs. Important structure–property relationships and trends were established through this comparison and processing-property relationships were also explored through variation in device annealing and determination of device stability upon exposure to air and bias stress. Oxygen-doping effects observed after prolonged exposure to air were also investigated using contact resistance measurements. Using eco-friendly materials such as carbohydrates and bio-inspired isoindigo, this new series of polymers demonstrates significantly improved device performance and both environmental and bias stress stability, all critical to commercialization of the next generation of organic electronics. This work serves as a model for the investigation of structure-processing-property relationships and the importance of these relationships to the optimization of electronic properties in SPs.

2. Results and Discussion

The synthetic route to the isoindigo-bithiophene statistical random copolymers, PiI-*n*-Ac and PiI-*n*-OH, is depicted in **Scheme 1**, with ***n*** referring to the number of carbons in the carbohydrate-containing side-chain spacer unit. A detailed experimental procedure for the synthesis of polymers PiI-*n*-Ac and PiI-*n*-OH is described in Supporting Information. Briefly, bromine-terminated alcohols with alkyl spacer chain lengths n = 4, 6, 8, 10, 12 carbons were reacted with β-D-galactose pentaacetate in the presence of boron trifluoride diethyl etherate. The crude side chains were then reacted directly with 6,6′-dibromoisoindigo to afford monomers **1**a-e in good yields (31–44%). Although synthetic procedures to access these polymers were previously reported,[30,31] the synthetic approach was revisited to improve the synthetic tunability (critical for expanding this approach to other saccharide units), to reduce side-product formation, and achieve overall higher yields. Notably, previous synthetic approaches often led to O-alkylation and other side-product formation that reduced synthetic yields and complicated purification. To address this synthetic challenge, the alkylation of the

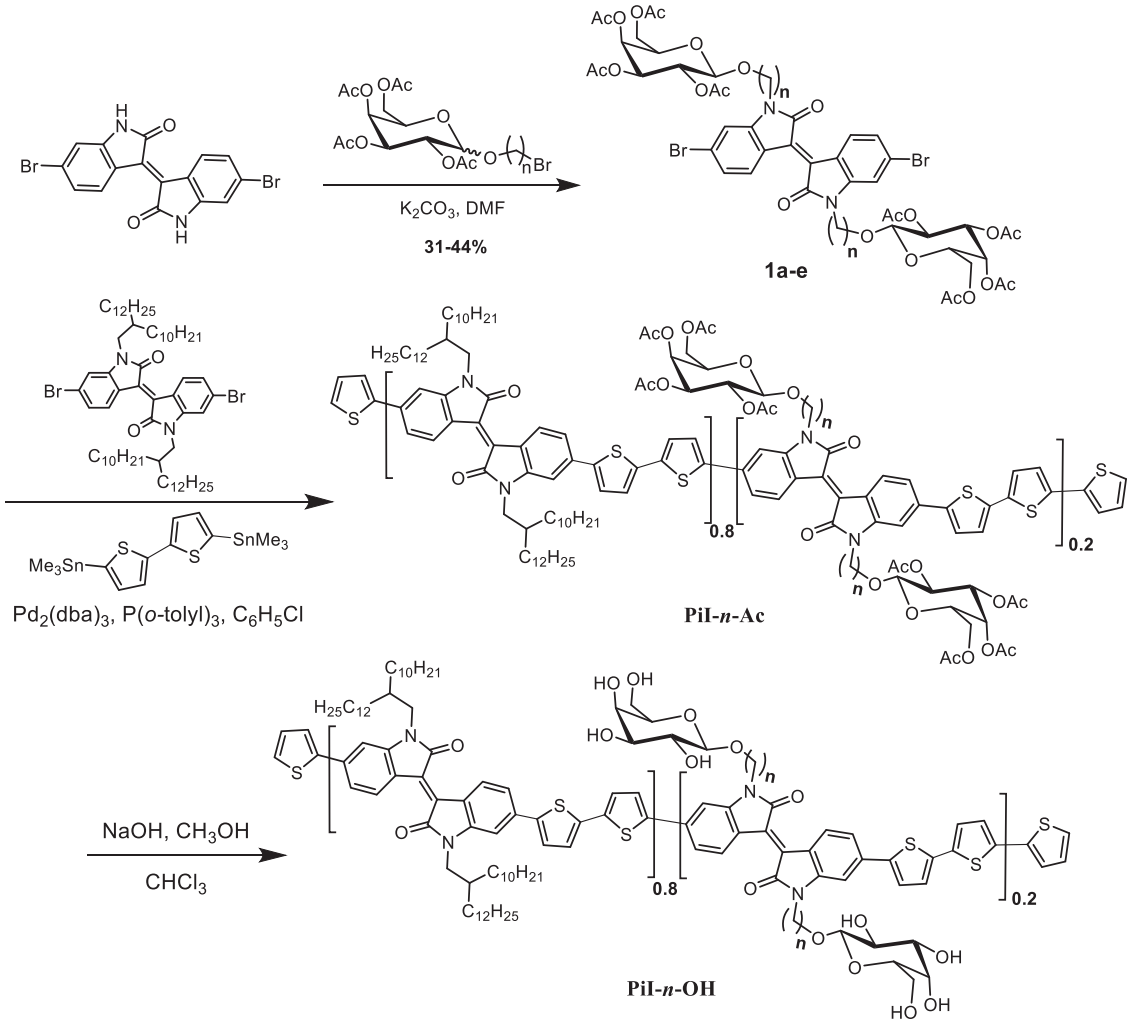

Scheme 1. Synthetic pathway for the preparation of semiconducting polymers PiI-*n*-Ac and PiI-*n*-OH.

isoindigo core with prefunctionalized side chains bearing galactose units was performed, which allowed for increased yields by preventing potential O-alkylation and for simpler purification via column chromatography on silica gel. Upon obtention of the different carbohydrate-containing monomers, statistical random copolymerization was performed via Stille cross-coupling polycondensation with monomers **1**a-e (20 mol%), (E)-6,6′-dibromo-1,1′-bis(2-decyltetradecyl)-[3,3′-biindolinylidene]-2,2′-dione (80 mol %) and 5,5′-bis(trimethylstannyl)-2,2′-bithiophene to afford acetyl-protected random copolymers PiI-*n*-Ac. Polymers PiI-*n*-OH were attained by removing the acetyl protecting groups according to previously reported basic conditions.[30]

Structural characterization of **1**a-e was carried out by ^{1}H NMR, ^{13}C NMR and mass spectrometry (see Supporting Information). Because the polymer series was generated through a random copolymerization method, the experimental ratios of the galactose-bearing monomer within the polymers were confirmed by ^{1}H NMR at 120 °C in 1,1,2,2-tetrachloroethane-d_2, as shown in Figure S1 (Supporting Information). A comparison of a chemical shift associated with the anomeric position of the carbohydrate unit (δ = 4.2 ppm) and the chemical shift associated with the isoindigo lactam ring (δ = 3.8 ppm) confirms that all polymers are composed of approximately 20% galactose-bearing isoindigo units. Furthermore, acetyl-deprotection to obtain PiI-*n*-OH was confirmed by Fourier-transform infrared (FTIR) spectroscopy. As shown in **Figure 1** and Figure S2 (Supporting Information), deprotection of the alcohol moieties is confirmed by loss of a C═O stretching peak at 1750 cm^{-1} associated with the acetyl protecting groups and the appearance of a broad O—H stretching band at 3370 cm^{-1}. Upon structural confirmation, the PiI-*n*-Ac and PiI-*n*-OH polymer series were further characterized by various methods, and the results are summarized in **Table 1**.

High-temperature size-exclusion chromatography was used to determine the molecular weight and polydispersity of the polymers. While most polymers were found to have similar molecular weights (around 20 kDa), PiI-4-Ac is slightly lower at 14 kDa. This is attributed to a decrease in solubility of both the monomer and resulting polymer arising from the short spacer chain between the isoindigo core and bulky carbohydrate end-group. Optical bandgap and λ_{max} of all polymers were determined using UV–Vis spectroscopy (Figure S3, Supporting Information). As shown in Table 1, the bandgaps are comparable for all polymers,

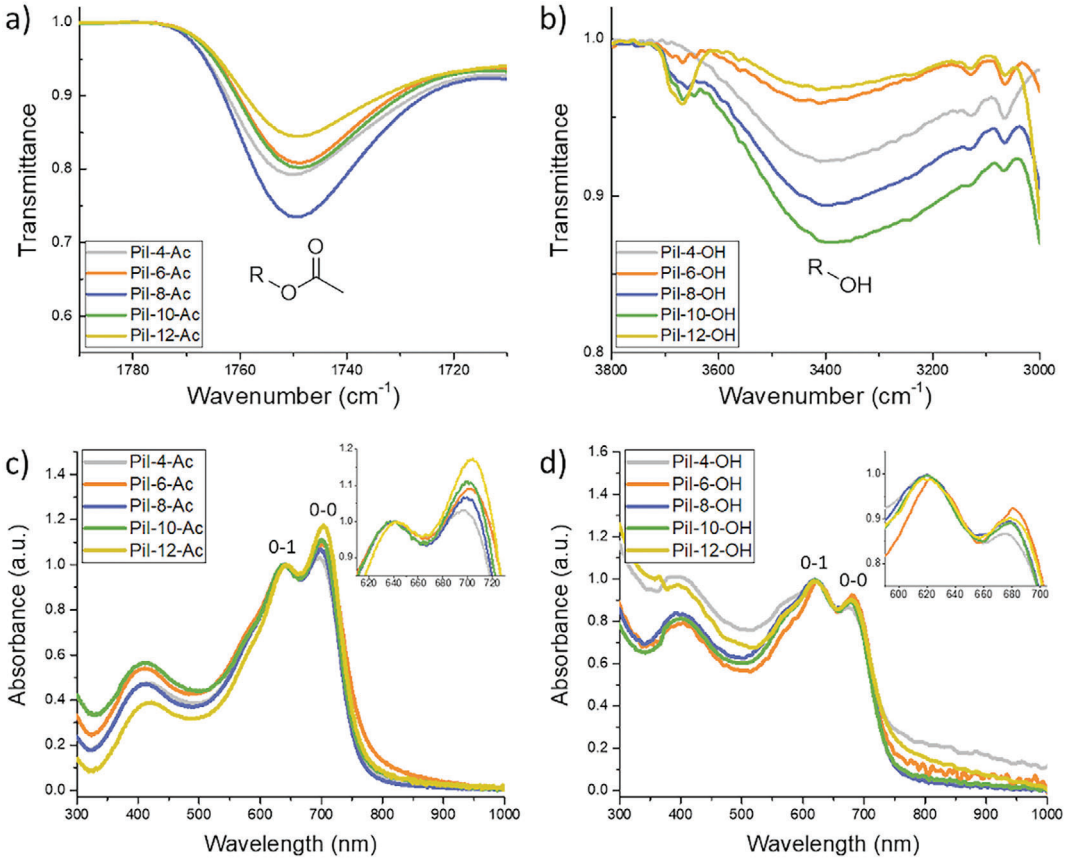

Figure 1. Characterization of the new polymers before and after acetyl deprotection. Fourier-transform infrared (FTIR) spectra of galactose-bearing polymers showing a) carbonyl and b) alcohol stretching peaks. Normalized UV–vis spectra of c) the PiI-*n*-Ac polymer series and d) the PiI-*n*-OH polymer series showing vibrational peaks 0–0 and 0–1.

indicating that the length of the side-chain spacer unit and polarity of the carbohydrate end-group do not significantly impact the electronic properties of the resulting polymers. The thermal stability of the polymers was also assessed by thermogravimetric analysis (TGA). As shown in Table 1 and Figure S5 (Supporting Information), thermal decomposition was measured for each polymer at 5% mass loss. All polymers had sufficiently high thermal stability at $T_d > 350$ °C.

The optical properties of the PiI-*n*-Ac and PiI-*n*-OH polymers were further characterized by thin-film UV–Vis spectroscopy. As

Table 1. Structural and optoelectronic characterization of the new isoindigo-based polymers. Measured molecular weights, polydispersity, optical properties, energy levels and thermal stability.

	M_n [kDa][a)]	M_w [kDa][a)]	$Đ$[b)]	$\lambda_{max\ (film)}$ [nm][c)]	E_g^{opt} [eV][d)]	T_d [°C][e)]
PiI-4-Ac	14.1	18.0	1.3	696	1.58	374
PiI-4-OH				683	1.59	375
PiI-6-Ac	21.9	35.8	1.6	700	1.56	377
PiI-6-OH				686	1.60	378
PiI-8-Ac	24.1	39.7	1.6	698	1.59	385
PiI-8-OH				685	1.61	381
PiI-10-Ac	22.0	38.1	1.7	700	1.57	386
PiI-10-OH				686	1.61	387
PiI-12-Ac	26.0	45.5	1.8	703	1.57	385
PiI-12-OH				684	1.59	386

[a)] Number-average molecular weight and weight-average molecular weight estimated by high temperature SEC in 1,2,4-trichlorobenzene at 180 °C using polystyrene as standard; [b)] Dispersity defined as M_w/M_n; [c)] Absorption maxima in thin film; [d)] Calculated by the following equation: gap = $1240/\lambda_{onset}$ of polymer film; [e)] Estimated from TGA at 5% mass loss.

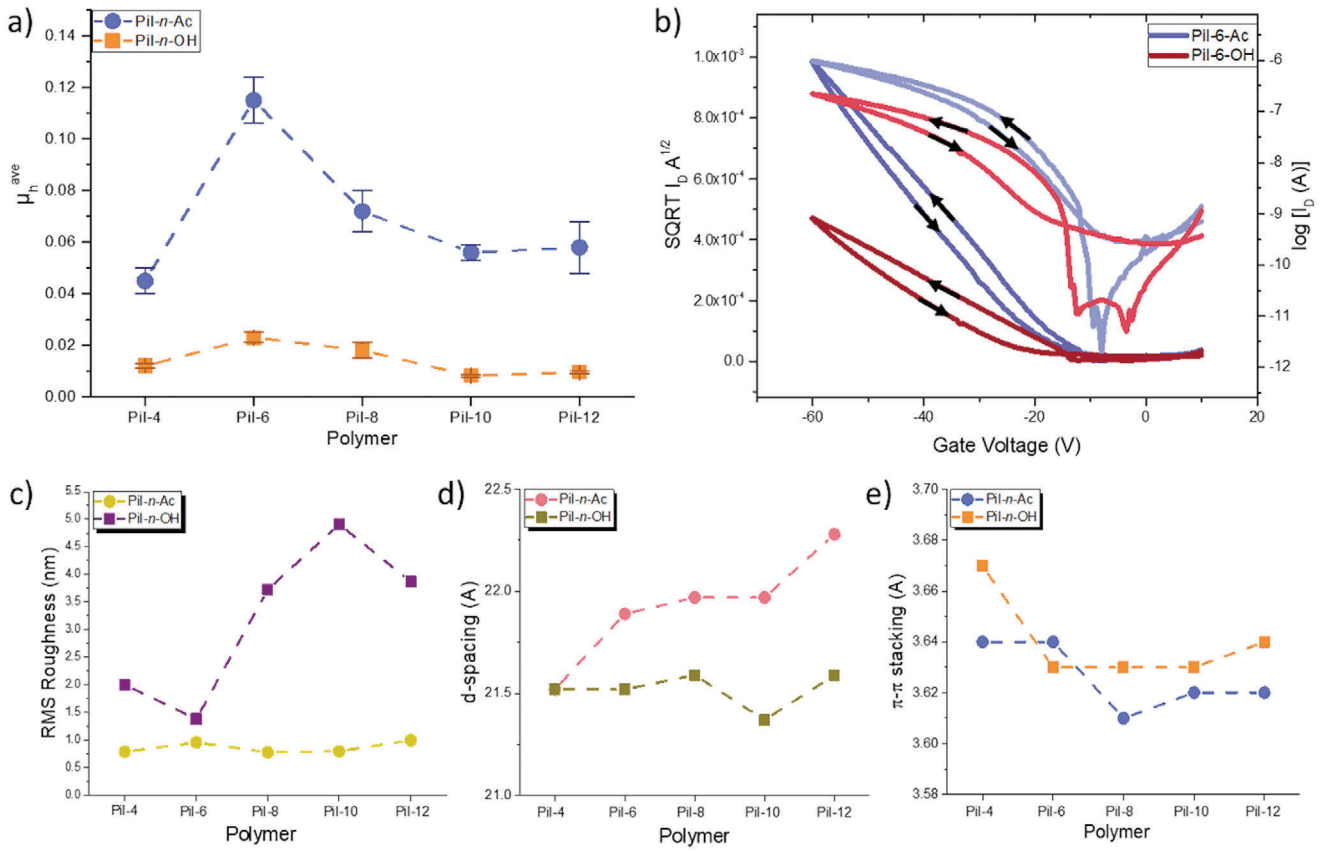

Figure 2. OFET characteristics of the new isoindigo-based polymers. a) Average hole mobilities of polymers PII-*n*-Ac and PII-*n*-OH with b) transfer curves of PII-6-Ac and PII-6-OH showing hysteresis behavior. Trends in c) RMS roughness measured by AFM, and d) d-spacing and e) π–π stacking measured from GIWAXS.

shown in Figure 1 and Figure S3 (Supporting Information), a broad absorption band attributed to donor-acceptor charge transfer in the polymer backbone can be observed centered at approximately $\lambda = 680$ nm. Comparison of the two vibrational peaks (0–0 and 0–1) of the absorption band gives insight to the solid-state aggregation behavior of the polymers.[34] As expected, the length of the side chain spacer has little impact on λ_{max} (associated with the effective conjugation length), but was found to impact solid-state aggregation. As noted in Figure 1c, aggregation increases with increasing side chain spacer length. The shorter chains and relatively bulky galactose end-groups can disrupt polymer chain interdigitation and aggregation compared to the longer chains, which allow for greater flexibility and closer packing of the polymer backbones. Additionally, a decrease in aggregation is observed in the PII-*n*-OH series compared to the PII-*n*-Ac series. This has been previously observed in conjugated polymers with hydrogen bonding side chains and indicates that the formation of intermolecular hydrogen bonding reduces aggregate formation by disrupting the stacking of polymer chains.[35]

Following material characterizations, these polymers were evaluated in OFETs. The full experimental procedure for the fabrication of the devices can be found in the Supporting Information. Briefly, devices with bottom-gate top contact configuration were prepared by spin-coating solutions of 5 mg mL^{-1} in 1,1,2,2-tetrachloroethane onto octyltrimethoxysilane (OTS) functionalized Si/SiO_2.[36] Physical vapor deposition was then used to deposit gold electrodes of various channel lengths and widths. Figures S6–S9 (Supporting Information) show the measured output and transfer curves of the PII-*n*-Ac and PII-*n*-OH polymer series, with key results summarized in Table S1 (Supporting Information). Linear fitting of $I_{DS}^{1/2}$ versus V_{GS} from the transfer curves in the saturation regime was used to extract charge carrier mobility (μ_{sat}) using the following equation:

$$I_{DS(sat)} = (WC/2L)\,\mu_{sat}\left(V_G - V_{th}\right)^2 \quad (1)$$

where I_{DS} is drain current, W and L are channel width and length, C is the dielectric constant of SiO_2, V_G is gate voltage and V_{th} is threshold voltage.

As shown in **Figure 2**a and Table S1 (Supporting Information), the field-effect mobilities measured for all polymers were similar, with the majority falling within the range of 10^{-2} cm^2 V^{-1} s^{-1}. While these results are not among the highest reported performances, comparable values have previously been published for similarly side chain engineered isoindigo-based polymers.[37,38] Importantly, all devices showed dramatically improved charge mobilities compared to our previous work. Previously, we synthesized isoindigo-based polymers bearing galactose side chains with two key structural differences: 1) a nine-carbon length side chain spacer between the isoindigo core and carbohydrate

end-group was used and 2) the isoindigo monomers were copolymerized with a thiophene donor.[30] When tested in OFETs, the highest average mobility of these polymers was found to be 2.3×10^{-4} cm^2 V^{-1} s^{-1}, significantly lower than the highest performance recorded in this work, 0.115 cm^2 V^{-1} s^{-1} (Table S1, Supporting Information). By using a more electron rich and planar donor, bithiophene, and even-numbered carbon spacer chains, the charge transport properties of carbohydrate-containing SPs in OFETs were improved by up to three orders of magnitude. It is important to note that odd-even effects in semiconducting polymer design and organic electronics are well-documented in the literature. Numerous examples have shown that even-numbered chain lengths typically lead to better side chain interdigitation and favorable chain packing, promoting enhanced crystallinity and charge hopping.[32,39–41] Therefore, our findings align with this established structural relationship, effectively exploiting the odd-even effects to enhance materials performance in device.[24,32]

By using a more electron rich and planar donor, bithiophene, and even-numbered carbon spacer chains, the charge transport properties of carbohydrate-containing SPs in OFETs were improved by up to three orders of magnitude. It is important to note that odd-even effects in semiconducting polymer design and organic electronics are well-documented in the literature. Numerous examples have shown that even-numbered chain lengths typically lead to better side-chain interdigitation and favorable chain packing, promoting enhanced crystallinity and charge hopping. Therefore, our findings align with this established structural relationship, effectively exploiting the odd-even effects to enhance materials performance in device.[24,32] Within each of the new polymer series, PiI-6-Ac and PiI-6-OH demonstrated the highest mobilities, with average values of 0.115 cm^2 V^{-1} s^{-1} and 0.023 cm^2 V^{-1} s^{-1}, respectively. The lowest charge mobility values measured from each series were for PiI-4-Ac (0.045 cm^2 V^{-1} s^{-1}) and PiI-10-OH (0.008 cm^2 V^{-1} s^{-1}). As shown in Figure 2a, the protected PiI-*n*-Ac polymers exhibit higher mobilities than the deprotected PiI-*n*-OH series by an average of fivefold. This is consistent with previous findings from our group and can be in part attributed to the charge-trapping sites generated by the exposure of the polar alcohol groups on the carbohydrate units of the PiI-*n*-OH series.[31,42,43] This charge trapping can also be observed through the increased hysteresis behavior in the transfer curves of the PiI-*n*-OH series compared to the PiI-*n*-Ac polymers (Figure 2b and Figures S7 and S9, Supporting Information). The PiI-*n*-Ac series also showed higher on/off current ratios and lower threshold voltages compared to the PiI-*n*-OH series.

To gain insight on thin-film morphologies and their impact on device characteristics, solid-state characterizations were performed with AFM and GIWAXS, with the results summarized in Table S2 (Supporting Information). AFM was used to investigate the surface microstructures and determine the root-mean-square (RMS) roughness of the polymer films. Height and phase images are shown in Figures S10 and S11 (Supporting Information). As shown in Figure 2c, the PiI-*n*-Ac series form smoother films than the PiI-*n*-OH polymers, with an average root-mean square (RMS) roughness of 0.87 nm for the PiI-*n*-Ac series compared to a much greater average value of 3.18 nm for the PiI-*n*-OH series. The increased roughness of the PiI-*n*-OH polymers can be attributed to a decrease in solubility resulting from hydrogen bonding between the carbohydrate side chains. The RMS roughness of the PiI-*n*-Ac series compared to that of the PiI-*n*-OH polymers is inversely related to the observed charge carrier mobilities, indicating that the smoother films yielded better-performing devices. Among the PiI-*n*-OH series, PiI-6-OH possesses the lowest RMS roughness, 1.38 nm, again correlating with the higher charge carrier mobility observed compared to the rest of the series. Among all devices, PiI-10-OH and PiI-12-OH show the highest RMS roughness (4.91 and 3.87 nm respectively) and lowest charge mobilities (0.008 and 0.009 cm^2 V^{-1} s^{-1}, respectively), further correlating film roughness with device performance. Since the RMS roughness was similar for all PiI-*n*-Ac polymers, ranging from 0.78 to 1.00 nm, surface morphology likely did not play a significant role in influencing device performance.

GIWAXS was used to further investigate the molecular packing of these polymers. 2D scattering patterns and 1D sector-averaged profiles are shown in Figures S12–S14 (Supporting Information).The d-spacing of the side chains (measured from the (100) peak) and π–π stacking of the polymer backbones (measured from the (010) peak) were determined and summarized in Table S2 (Supporting Information). As shown in Figure 2d and d-spacing for the PiI-*n*-OH series was found to be closer than that of the PiI-*n*-Ac series, with average distances of 21.52 and 21.93 Å for each series respectively. This is consistent with our previous works and indicates that the hydrogen bonding between the exposed alcohol groups of the carbohydrate units leads to closer packing of the side chains.[31] Interestingly, side chain length does not appear to have significant impact on *d*-spacing in the PiI-*n*-OH series. Conversely, when the alcohol units are not exposed in the PiI-*n*-Ac series, spacer chain length bears a more substantial impact on d-spacing, with increasing chain length more closely correlated to greater spacing between side chains due to the bulky carbohydrate end-groups and an absence of hydrogen bonding to draw them together (Figure 2d). When compared to our previous work, the odd-even effect can be seen by the closer packing of these polymer side chains. In our previous work using an odd numbered spacer chain ($n = 9$), we observed a d-spacing of 24.17 Å. This distance is significantly larger than any of the polymers in this work, whose largest *d*-spacing distances ranged from 21.37 to 22.28 Å.[30] Furthermore, no higher-order reflections were observed for the previous works, while both (200) and (300) reflections were observed for nearly all of the PiI-*n*-Ac series and several of the PiI-*n*-OH series (Figures S12 and S13, Supporting Information), indicating that the changes in polymer backbone structure and side chain spacer in this new series of materials significantly improve long-range order in solid-state. Notably, these polymers all showed π–π stacking in only the in-plane direction (Figures S12–S14, Supporting Information), signifying that the polymer chains pack in an edge-on orientation relative to the substrate, which has been reported to be more favorable compared to face-on orientation for device performance in OFETs.[44]

To probe the effects of annealing on device performance, PiI-6-Ac was chosen to fabricate OFETs annealed at several different temperatures. The output and transfer characteristics are shown in Figures S15 and S16 (Supporting Information), with the results summarized in Table S3 (Supporting Information). Thin films were annealed at 150 and 200 °C for 30 min each to

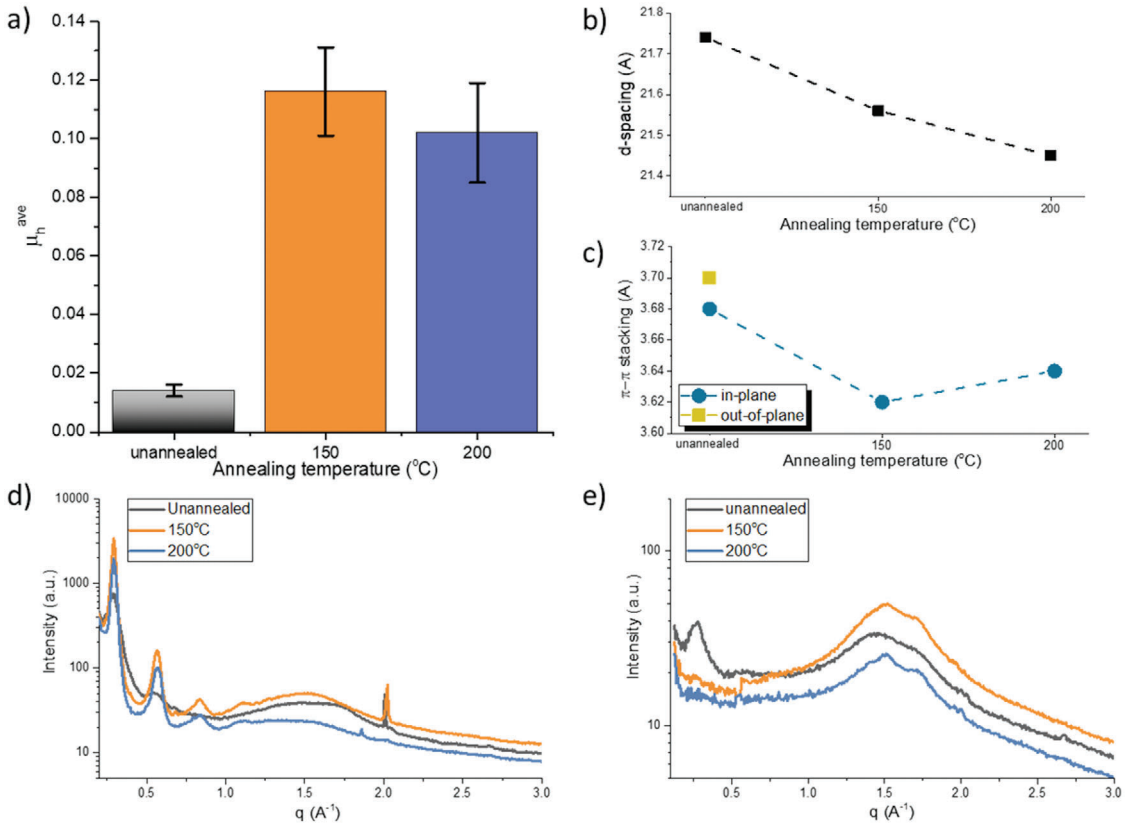

Figure 3. Characteristics of PiI-6-Ac under varied annealing conditions. a) Average hole mobilities, b) d-spacing, and c) π–π stacking of PiI-6-Ac after annealing at various temperatures. 1D sector-averaged profiles of PiI-6-Ac annealed at various temperatures in d) out-of-plane and e) in-plane directions. Note that the sharp peaks at ≈ 2 Å^{-1} in d) is attributed to impurities.

determine whether variation in annealing temperature plays a significant role in the improvement of device performance. An unannealed device was also tested to determine how annealing impacts the performance and morphology of the polymer. Interestingly, it was found that annealing temperature does not play a significant role in device performance, with similar charge mobilities measured at both annealing temperatures. The average values obtained for devices annealed at 150 °C (0.116 cm^2 V^{-1} s^{-1}) and 200 °C (0.102 cm^2 V^{-1} s^{-1}) were found to be within each other's standard deviations, and within that of the initial PiI-6-Ac device (0.115 cm^2 V^{-1} s^{-1}), which was annealed at 175 °C for 30 min. As shown in **Figure 3**a, these values were significantly higher than the charge mobility of the unannealed device, which showed an average charge mobility of only 0.014 cm^2 V^{-1} s^{-1}, a full order of magnitude lower than the annealed devices. The substantial improvement in charge mobility measured after annealing can be correlated to changes in molecular packing, observed through GIWAXS. 1D sector-averaged profiles shown in Figure 3d,e, with 2D scattering patterns in Figure S17 (Supporting Information) and calculated values in Table S4 (Supporting Information). As shown in Figure 3 and Table S4 (Supporting Information), the thermally annealed devices show closer packing of both side chains and polymer backbones compared to the unannealed device. Notably, the impact of annealing on long-range order and packing orientation is much more significant. The unannealed film lacks a (300) reflection compared to the annealed samples and exhibits both in-plane and out-of-plane π–π stacking. Upon thermal annealing, the samples exhibited improved long-range order and transitioned to a more edge-on orientation relative to the substrate. This enhancement in long-range order and preferable reorientation of the polymer chains to edge-on packing upon thermal annealing, previously observed in similar semiconducting polymers, support the observed significant increase in charge mobility after annealing the devices.[34,45]

An important consideration for expanding the application of organic electronics is stability in environmental conditions in which the device may be used. SPs often exhibit poor stability when exposed to oxygen and moisture.[8,46] For this reason, the majority of reported charge mobilities are measured in controlled environments from devices fabricated in air-free conditions. To investigate the air stability of the PiI-*n*-Ac and PiI-*n*-OH polymer series, OFETs were fabricated and tested after exposure to ambient conditions for various lengths of time. The fabrication of these devices was conducted in completely air-free conditions in an N_2-filled glovebox. This contrasts with the previously discussed results, where the solution preparation and spin-coating steps of device fabrication were conducted in open-air conditions. By fabricating the devices in a completely air-free environment, a baseline could be established to determine the effects of air exposure over time. For each polymer, devices were tested on the same substrate in pristine (air-free) conditions, then after successive exposure to ambient air for 24 h, 72 h, and 10 days (240 h).

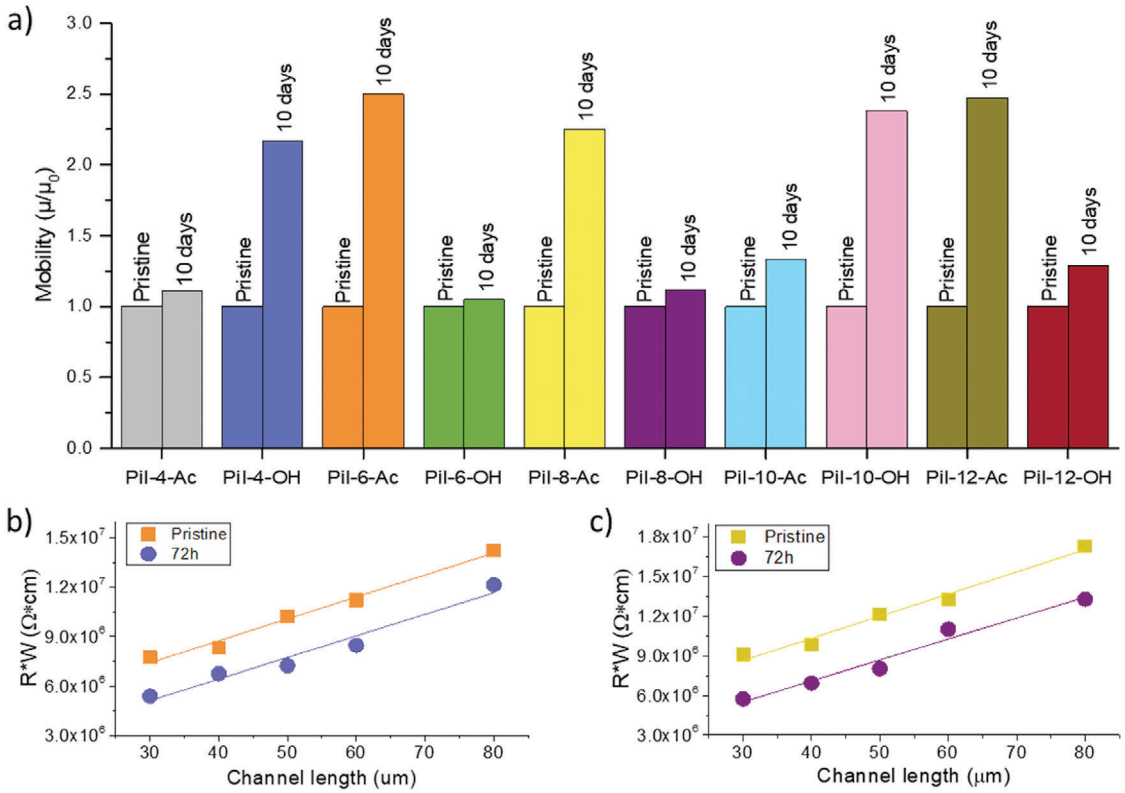

Figure 4. OFET characteristics of the new isoindigo-based polymers upon exposure to air. a) Charge carrier mobilities (extracted from the transfer characteristics in the saturation regime) in air-free (pristine) conditions, then after exposure to air for 10 days, normalized to $\mu_{pristine} = 1$. Width-normalized resistance (R^*W) of polymers b) PiI-4-Ac and c) PiI-12-Ac calculated from devices of various channel lengths in the linear regime. Line-of-best-fit used to calculate the width-normalized contact resistance.

The transfer characteristics of these devices are shown in Figures S18–S21 (Supporting Information) with the results summarized in Table S5 (Supporting Information).

As shown in **Figure** 4a, these polymers all possess excellent air stability, with no degradation of charge mobility after 10 days of exposure to ambient air. On/off current ratios were also maintained after 10 d of air exposure (Figures S18 and S20, Supporting Information). Surprisingly, the charge carrier mobilities improved after prolonged exposure to air by as much as 2.5 times that of the pristine values. Additionally, the transfer curves demonstrate more ideal behavior after exposure to air. As shown in Figures S19 and S21 (Supporting Information), the square-root curves become more linear with increasing exposure to air. Interestingly, similar observations of increased charge mobility and device stability upon exposure to air over time were reported with an indacenodithiophene-co-benzothiadiazole polymer, in which these effects were attributed to oxygen diffusion and doping.[47] Incidental exposure to oxygen in air is known to *p*-dope some organic semiconductors through various charge transfer mechanisms.[48–52] The significant improvement of measured charge mobilities observed in these devices after exposure to air can therefore be attributed to incidental oxygen-doping effects. Notably, upon exposure to ambient air (and hence oxygen, but also variable humidity), the threshold voltages of the devices also changed, with some devices exhibiting significant threshold voltage shifts. Considering that the threshold voltage is highly sensitive to doping and is influenced by charge traps and limitations in charge injection, the observed variations are likely caused by exposure to humidity, which allows water to diffuse into the devices, leading to water-related charge traps.[53–56] Additionally, decreased contact resistances can lead to improved charge injection, potentially causing shifts in the threshold voltage toward zero gate-source bias.[57] We anticipate that both effects are present simultaneously.

To investigate the increase in OFET performance observed after exposure to air, the width-normalized contact resistance (R_cW) was determined in pristine (air-free) devices, then after exposure to ambient air for 72 hours for two representative polymers. Contact resistance can be affected by doping through improvement of charge injection at the metal–semiconductor interface.[48,57,58] Therefore, changes observed in contact resistance after exposure to air can be correlated to incidental oxygen doping effects. Since all polymers show similar trends of increasing performance over time, PiI-4-Ac and PiI-12-Ac, polymers at each extreme of the series, were chosen for this experiment.

Width-normalized contact resistance was calculated for devices from polymers PiI-4-Ac and PiI-12-Ac in pristine conditions and after exposure to air for 72 hours using the transmission line method (TLM) according to previous reports.[58–61] This method is based on the assumption that, in the linear regime, the total resistance of a transistor is the sum of the channel resistance and the contact resistance. As shown in Figure 4b,c, by

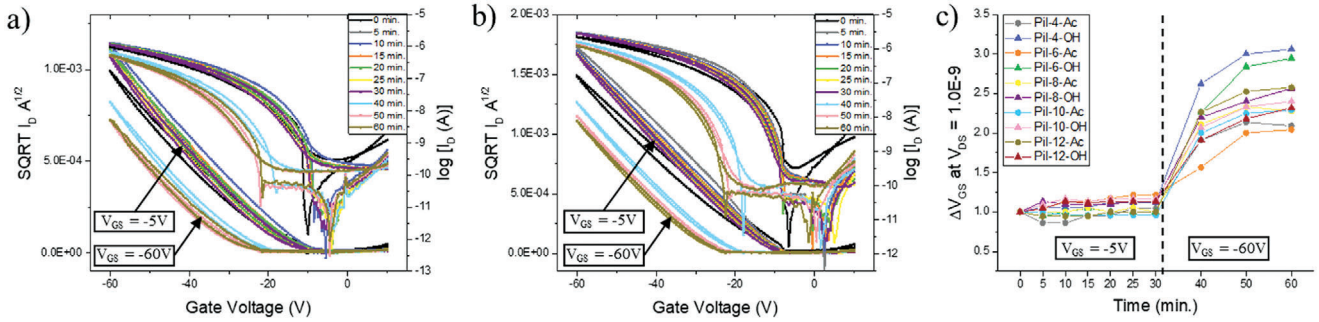

Figure 5. OFET characteristics of PiI-4-Ac and PiI-4-OH under bias stress. Transfer curves of a) PiI-4-Ac and b) PiI-4-OH under bias stress conditions: $V_{GS} = -5$ V, $V_{DS} = -60$ V for 30 minutes with transfer curves measured at 5 minute intervals, then $V_{GS} = V_{DS} = -60$ V for an additional 30 minutes with transfer curves measured at 10 minute intervals. Inset arrows indicate transfer curves measured at each set of stress conditions. c) Change in gate voltage at a set source–drain current ($I_{DS} = 1 \times 10^{-9}$) of all devices versus time under bias stress.

plotting the width-normalized resistance against channel lengths ranging from 30 to 80 μm, the total resistance can be extrapolated to a channel length of 0, effectively eliminating contributions of channel resistance to total resistance. In other words, the total resistance at a channel length of 0 is an estimate of the contact resistance. Total resistance (R) for each device was calculated using the drain current (I_D) at a set overdrive voltage ($V_{GS} - V_{th} = -20$ V) and a fixed drain voltage ($V_{DS} = -5$ V), then normalized by channel width (W) according to the following equation: $R^*W = (I_D/V_{DS})\ W$. As shown in Figure 4 and Table S6 (Supporting Information), the contact resistance decreases significantly upon exposure to air for both the PiI-4-Ac and PiI-12-Ac devices by approximately threefold (from 3.61×10^6 to 0.82×10^6 Ω cm and 3.41×10^6 to 1.14×10^6 Ω cm respectively), in agreement with the observed increases in charge mobilities after prolonged exposure to air. This result supports the conclusion that the increased performance of these devices observed after prolonged exposure to air is the result of incidental oxygen doping. Additionally, when comparing PiI-4-Ac to PiI-12-Ac, the contact resistance values are very similar, indicating that the side chain structure has a negligible effect on the resistance and oxygen doping effects of the devices.

To further probe other aspects of the stability of these polymers in OFETs, bias stress measurements were conducted with the results summarized in **Figure 5** and Figures S22 and S23 (Supporting Information). The bias stress stability of these devices was tested by first applying a constant source-gate voltage of –5 V and source–drain voltage of –60 V for a total of 30 min, with transfer curves ($V_{DS} = -60$ V, $V_{GS} = 10$ to –60 V) measured at 5 min intervals. A constant source–gate voltage of –60 V and source–drain voltage of –60 V were then applied for an additional 30 minutes, with transfer curves ($V_{DS} = -60$ V, $V_{GS} = 10$—60 V) measured at 10 min intervals. Importantly, the devices remained stable, with no significant changes to the transfer characteristics after 30 min of mild stress. Upon increase of the bias stress voltage, a threshold shift was observed for all devices, a commonly observed phenomenon in conjugated polymer OFETs.[62,63] However, the thresholds did not continue to shift significantly after the initial increase in bias stress voltage and began to plateau again. Interestingly, when comparing changes in gate voltage at a set source-drain current versus time (Figure 5c), the acetyl protected polymers with shorter chains (PiI-4-Ac and PiI-6-Ac) showed significantly reduced bias stress effects at higher voltages compared to their deprotected counterparts (PiI-4-OH and PiI-6-OH). As the side chains increased, the difference in bias stress stability appears to decrease. This indicates that the polarity of the carbohydrate groups only affects bias stress stability significantly when coupled with shorter side chain spacers. These results indicate that the carbohydrate-containing polymers are not only stable to ambient environmental conditions, but can also be tuned to achieve variable resistance to bias stress effects.

3. Conclusions

In summary, we have developed two series of isoindigo-based polymers with galactose side chains containing varied alkyl spacer lengths (PiI-*n*-Ac and PiI-*n*-OH) to investigate structure–processing-property relationships toward the enhancement of device performance. Upon structural characterization, these polymers were used as active layers in OFETs to determine their electronic properties. Compared to our previous works, these polymers exhibited dramatically improved charge mobilities by up to three orders of magnitude. Investigation of thin film characteristics revealed that the PiI-*n*-OH series displays closer *d*-spacing than the PiI-*n*-Ac series, resulting from hydrogen bonding. However, the PiI-*n*-OH series also show greater film roughness and poorer device performance compared to the PiI-*n*-Ac series. By contrast, the PiI-*n*-Ac series had smoother films and closer π–π stacking, accounting for the observed increase in charge mobility. Both series exhibit favorable edge-on orientation of the polymer backbones and long-range order, observed by GIWAXS. Interestingly, though thermal annealing temperature had little effect on device performance, annealing was crucial to achieve favorable orientation and long-range order, leading to an increase in charge mobility by an order of magnitude compared to unannealed devices. Furthermore, the polymers all demonstrated excellent environmental stability. Upon exposure to ambient air for 10 days, the polymers showed substantial improvement of device performance in OFETs by up to 2.5 times, resulting from incidental oxygen doping. The doping effects were correlated to a reduction in contact resistance by approximately threefold in devices after exposure to air. These polymers also demonstrated good bias stress stability, with the shorter acetyl-protected chains showing the greatest reduction of bias stress effects. This work presents

an important model for the investigation and optimization of device performance in sidechain engineered semiconducting polymers. Notably, there are many possible paths to be explored in future work to further improve device performance, including optimization of the fabrication processes through automated high-throughput platforms, artificial intelligence, or asymmetric side chain engineering.[15,64–66] Nonetheless, carbohydrate-containing semiconducting polymers, due to their potential biocompatibility, their green solvent processability, good device performance, and excellent air stability, open new avenues to bridge a critical gap toward the commercialization of next-generation organic electronics.

Supporting Information

Supporting Information is available from the Wiley Online Library or from the author.

Acknowledgements

The authors thank Jean-François Morin and his group (U. Laval) for MS measurements, and Max Planck Institute for Polymer Research (Mainz, Germany) for the use of their facilities. This research used beamline 7.3.3 of the Advanced Light Source, a DOE Office of Science User Facility under contract DE-AC02-05CH11231. This work was supported by NSERC through a Discovery Grants (RGPIN-2017-06611) and the NSERC Green Electronics Network (GreEN) (NETGP 508526-17). S.R.-G. also acknowledges the Canada Foundation for Innovation (CFI), the Ontario Research Fund, and the University of Windsor for financial support. M.M. thanks NSERC for financial support through a Canada Postgraduate Scholarship - Doctoral. Y.W. and X.G. thank the National Science Foundation under award number DMR-2047689 for financial support of morphology characterizations. This research used beamline 7.3.3 of the Advanced Light Source, which is a DOE Office of Science User Facility under contract no. DE-AC02-05CH11231. Y.W. was supported in part by an ALS Doctoral Fellowship in Residence. Table of content graph was created using BioRender (L. Pandolfi 2024, BioRender.com/j88q959

Conflict of Interest

The authors declare no conflict of interest.

Author Contributions

All authors contributed to the manuscript. All authors have given approval to the final version of the manuscript.

Data Availability Statement

The data that support the findings of this study are available from the corresponding author upon reasonable request.;

Keywords

green materials, organic electronics, organic field-effect transistors, semiconducting polymers, side-chain engineering

Received: August 16, 2024
Published online:

[1] A. Bunea, V. Dediu, E. A. Laszlo, F. Pistri, F. S. Iliescu, O. N. Ionescu, *Micromachines* **2021**, *12*, 1091.
[2] J. S. Heo, J. Eom, Y. Kim, S. K. Park, *Small* **2018**, *14*, 1703034.
[3] D. Schaefer, W. M. Cheung, *Proc. CIRP* **2023**, *72*, 1022.
[4] *Organic Semiconductors in Sensor Applications* (Eds: D. A. Bernards, R. M. Owens, G. G. Malliaras) Springer-Verlag, Berlin **2008**.
[5] J. Rivnay, R. M. Owens, G. G. Malliaras, *Chem. Mater.* **2014**, *26*, 679.
[6] D. Corzo, G. Tostado-blázquez, D. Baran, *Front. Electron.* **2020**, *1*, 594003.
[7] M. H. Gharahcheshmeh, K. K. Gleason, *Energies* **2022**, *15*, 3661.
[8] A. J. Heeger, *Chem. Soc. Rev.* **2010**, *39*, 2354.
[9] S. Lv, L. Li, Y. Mu, X. Wan, *Polym. Rev.* **2021**, *61*, 520.
[10] Y. Zhou, L. Li, Z. Han, Q. Li, J. He, Q. Wang, *Chem. Rev.* **2023**, *123*, 558.
[11] M. U. Ocheje, B. P. Charron, A. Nyayachavadi, S. Rondeau-Gagné, *Flex. Print. Electron.* **2017**, *2*, 043002.
[12] S. Holliday, J. E. Donaghey, I. McCulloch, *Chem. Mater.* **2014**, *26*, 647.
[13] A. F. Paterson, S. Singh, K. J. Fallon, T. Hodsden, Y. Han, B. C. Schroeder, H. Bronstein, M. Heeney, I. McCulloch, T. D. Anthopoulos, A. F. Paterson, I. McCulloch, T. D. Anthopoulos, S. Singh, B. C. Schroeder, K. J. Fallon, H. Bronstein, T. Hodsden, Y. Han, M. Heeney, *Adv. Mater.* **2018**, *30*, 1801079.
[14] M. Mooney, C. Crep, S. Rondeau-Gagné, *ACS Appl. Electron. Mater.* **2022**, *4*, 5652.
[15] M. Mooney, A. Nyayachavadi, A. Awada, E. Iakovidis, Y. Wang, M. N. Chen, Y. Liu, J. Xu, Y. C. Chiu, X. Gu, S. Rondeau-Gagné, *Polym. Chem.* **2022**, *14*, 562.
[16] A. Hakami, S. S. Srinivasan, P. K. Biswas, A. Krishnegowda, S. L. Wallen, E. K. Stefanakos, *J. Coat. Technol. Res.* **2022**, *19*, 377.
[17] K. Nakabayashi, T. Takahashi, R. Sugawara, C. T. Lo, H. Mori, *React. Funct. Polym.* **2018**, *131*, 350.
[18] N. Yousefi, C. Caba, A. Hu, M. Mooney, S. Zhang, A. D. Agostinis, M. Mirhassani, M. J. Ahamed, Y. Tong, S. Rondeau-Gagné, *ACS Appl. Electron. Mater.* **2022**, *4*, 4972.
[19] S. Ogawa, *Organic Electronics Materials and Devices*, Springer, Berlin **2015**.
[20] Y. Loo, I. Mcculloch, *MRS Bull.* **2008**, *33*, 653.
[21] L. Luok, W. Huang, C. Yang, J. Zhang, Q. Zhang, *Front. Phys.* **2021**, *16*, 33500.
[22] H. Bronstein, C. B. Nielsen, B. C. Schroeder, I. McCulloch, *Nat. Rev. Chem.* **2020**, *4*, 66.
[23] M. J. Kim, A. R. Jung, M. Lee, D. Kim, S. Ro, S. M. Jin, H. D. Nguyen, J. Yang, K. K. Lee, E. Lee, M. S. Kang, H. Kim, J. H. Choi, B. Kim, J. H. Cho, *ACS Appl. Mater. Interfaces* **2017**, *9*, 40503.
[24] F. Tao, S. L. Bernasek, *Chem. Rev.* **2007**, *107*, 1408.
[25] P.-O. Morin, T. Bura, M. Leclerc, *Mater. Horiz.* **2016**, *3*, 11.
[26] A. Teichler, J. Perelaer, U. S. Schubert, *J. Mater. Chem. C* **2013**, *1*, 1910.
[27] J. Yang, Z. Zhao, S. Wang, Y. Guo, Y. Liu, *Chem* **2018**, *4*, 2748.
[28] C. A. Di, K. Lu, L. Zhang, Y. Liu, Y. Guo, X. Sun, Y. Wen, G. Yu, D. Zhu, *Adv. Mater.* **2010**, *22*, 1273.
[29] V. Chaudhary, R. K. Pandey, R. Prakash, N. Kumar, A. K. Singh, *Synth. Met.* **2019**, *258*, 116221.
[30] M. Mooney, Y. Wang, A. Nyayachavadi, S. Zhang, X. Gu, S. Rondeau-Gagné, *ACS Appl. Mater. Interfaces* **2021**, *13*, 25175.
[31] M. Mooney, Y. Wang, E. Iakovidis, X. Gu, S. Rondeau-Gagné, *ACS Appl. Electron. Mater.* **2021**, *4*, 1381.
[32] H. Yu, K. H. Park, I. Song, M. J. Kim, Y. H. Kim, J. H. Oh, *J. Mater. Chem. C* **2015**, *3*, 11697.
[33] T. Lei, Y. Cao, X. Zhou, Y. Peng, J. Bian, J. Pei, *Chem. Mater.* **2012**, *24*, 1762.
[34] B. C. Schroeder, T. Kurosawa, T. Fu, Y. C. Chiu, J. Mun, G. J. N. Wang, X. Gu, L. Shaw, J. W. E. Kneller, T. Kreouzis, M. F. Toney, Z. Bao, *Adv. Funct. Mater.* **2017**, 27.

[35] M. U. Ocheje, B. P. Charron, Y. H. Cheng, C. H. Chuang, A. Soldera, Y. C. Chiu, S. Rondeau-Gagné, *Macromolecules* **2018**, *51*, 1336.
[36] G. C. Yuan, Z. Xu, C. Gong, Q. J. Cai, Z. S. Lu, J. S. Shi, F. J. Zhang, S. L. Zhao, N. Xu, C. M. Li, *Appl. Phys. Lett.* **2009**, *94*, 153308.
[37] N. M. Randell, T. L. Kelly, *Chem. Rec.* **2019**, *19*, 973.
[38] N. Luo, P. Ren, Y. Feng, X. Shao, H. L. Zhang, Z. Liu, *J. Phys. Chem. Lett.* **2022**, *13*, 1131.
[39] E. K. Burnett, B. P. Cherniawski, S. J. Rosa, D. Smilgies, S. Parkin, A. L. Briseno, *Chem. Mater.* **2018**, *30*, 2550.
[40] T. Lei, J. Wang, J. Pei, *Chem. Mater.* **2014**, *26*, 594.
[41] J. Y. Back, H. Yu, I. Song, I. Kang, H. Ahn, T. J. Shin, S. Kwon, J. H. Oh, Y. Kim, *Chem. Mater.* **2015**, *27*, 1732.
[42] D. Duarte, D. Sharma, B. Cobb, A. Dodabalapur, *Appl. Phys. Lett.* **2011**, *98*, 133302.
[43] S. Kim, H. Yoo, J. Choi, *Sensors* **2023**, *23*, 2265.
[44] M. Saito, T. Koganezawa, I. Osaka, *Appl. Polym. Mater.* **2019**, *1*, 1257.
[45] A. Luzio, J. Martin, C. H. Cheng, N. Stingelin, M. F. Toney, A. Salleo, M. Caironi, *J. Mater. Chem. C* **2021**, *9*, 15848.
[46] S. Griggs, A. Marks, H. Bristow, I. McCulloch, *J. Mater. Chem. C* **2021**, *9*, 8099.
[47] I. Dobryden, V. V. Korolkov, V. Lemaur, M. Waldrip, H. I. Un, D. Simatos, L. J. Spalek, O. D. Jurchescu, Y. Olivier, P. M. Claesson, D. Venkateshvaran, *Nat. Commun.* **2022**, *13*, 3076.
[48] B. Lüssem, C. M. Keum, D. Kasemann, B. Naab, Z. Bao, K. Leo, *Chem. Rev.* **2016**, *116*, 13714.
[49] M. S. A. Abdou, F. P. Orfino, Y. Son, S. Holdcroft, *J. Am. Chem. Soc.* **1997**, *119*, 4518.
[50] C. K. Lu, H. F. Meng, *Phys. Rev. B: Condens. Matter Mater. Phys.* **2007**, *75*, 2.
[51] D. R. Hines, V. W. Ballarotto, E. D. Williams, Y. Shao, S. A. Solin, *J. Appl. Phys.* **2007**, *101*, 024503.
[52] P. K. Nayak, R. Rosenberg, L. Barnea-Nehoshtan, D. Cahen, *Org. Electron.* **2013**, *14*, 966.
[53] Z. Jagoo, L. E. McNeil, *Adv. Mater. Interfaces* **2024**, *11*, 2301088.
[54] Y. Zhu, Y. Zhang, J. Yu, C. Zhou, C. Yang, L. Wang, L. Wang, L. Ma, L. J. Wang, *Sens. Actuators, B* **2023**, *374*, 132815.
[55] H. F. Haneef, A. M. Zeidell, O. D. Jurchescu, *J. Mater. Chem. C* **2020**, *8*, 759.
[56] M. Nikolka, G. Schweicher, J. Armitage, I. Nasrallah, C. Jellett, Z. Guo, M. Hurhangee, A. Sadhanala, I. McCulloch, C. B. Nielsen, H. Sirringhaus, *Adv. Mater.* **2018**, *30*, 1801874.
[57] A. D. Scaccabarozzi, A. Basu, F. Aniés, J. Liu, O. Zapata-Arteaga, R. Warren, Y. Firdaus, M. I. Nugraha, Y. Lin, M. Campoy-Quiles, N. Koch, C. Müller, L. Tsetseris, M. Heeney, T. D. Anthopoulos, *Chem. Rev.* **2022**, *122*, 4420.
[58] Z. A. Lamport, H. F. Haneef, S. Anand, M. Waldrip, O. D. Jurchescu, *J. Appl. Phys.* **2018**, *124*, 071101.
[59] F. Ante, D. Kälblein, U. Zschieschang, T. W. Canzler, A. Werner, K. Takimiya, M. Ikeda, T. Sekitani, T. Someya, H. Klauk, *Small* **2011**, *7*, 1186.
[60] U. Kraft, J. E. Anthony, E. Ripaud, M. A. Loth, E. Weber, H. Klauk, *Chem. Mater.* **2015**, *27*, 998.
[61] U. Kraft, K. Takimiya, M. J. Kang, R. Rödel, F. Letzkus, J. N. Burghartz, E. Weber, H. Klauk, *Org. Electron.* **2016**, *35*, 33.
[62] M. Nikolka, I. Nasrallah, B. Rose, M. K. Ravva, K. Broch, A. Sadhanala, D. Harkin, J. Charmet, M. Hurhangee, A. Brown, S. Illig, P. Too, J. Jongman, I. Mcculloch, J. Bredas, *Nat. Mater.* **2017**, *16*, 356.
[63] S. Park, S. H. Kim, H. H. Choi, B. Kang, K. Cho, *Adv. Funct. Mater.* **2020**, *30*, 1904590.
[64] A. Vriza, H. Chan, J. Xu, *Chem. Mater.* **2023**, *35*, 3046.
[65] Z. Tang, X. Xu, R. Li, L. Yu, L. Meng, Y. Wang, Y. Li, Q. Peng, *ACS Appl. Mater. Interfaces* **2020**, *12*, 17760.
[66] Y. C. Lin, F. H. Chen, Y. C. Chiang, C. C. Chueh, W. C. Chen, *ACS Appl. Mater. Interfaces* **2019**, *11*, 34158.